



POLITECNICO  
MILANO 1863

## Modelling and control of a Magnetic Levitation System

---

Tommaso Bocchietti 10740309

Daniele Cianca 10764733

Sara Orazzo 10995845

December 19, 2024

Politecnico di Milano

# Agenda

1. Introduction
2. Modelling
3. Parameters identification
4. Model Analysis
5. Estimators and Filters Design
6. Controllers design
7. Results
8. Conclusions



**Figure 1:** Magnetic Levitation System and its components

## **Introduction**

---

# Magnetic Levitation System (MLS)

Magnetic Levitation System (MLS) is an electromechanical system that enhances magnetic fields to levitate a ferromagnetic object. It's known for its non-linear behavior and its instability.

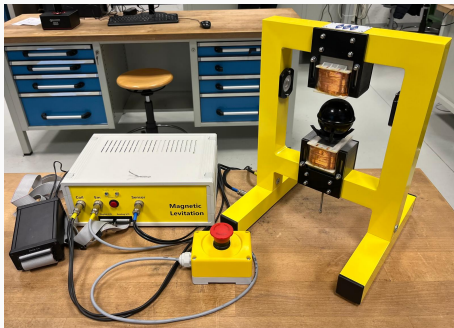


**Figure 2:** Magnetic Levitation System used in this work.

The variable magnetic field is generated by two electromagnets driven in voltage, while the position of the ball is measured by an optical infrared sensor.

## Project objectives

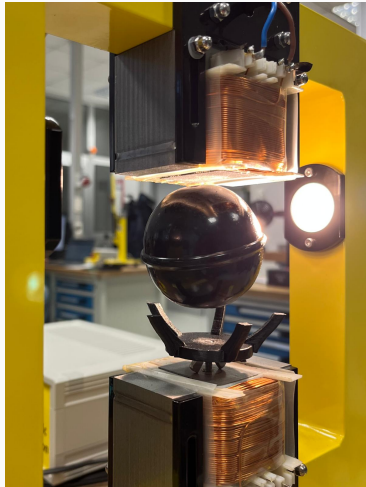


**Figure 3:** Sphere levitating

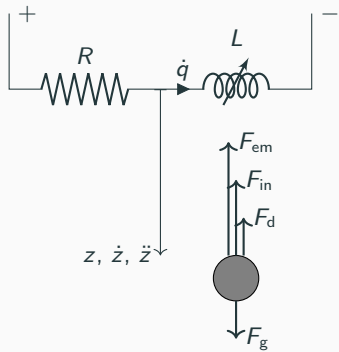
Project objectives:  
**Make the ball levitate.**

## **Modelling**

---

## Scheme of MLS system

Even if MLS is composed of two coils, for the aim of this work we have chosen to focus on the **single coil configuration**, considering only the upper one.



Name	Description
$F_g$	Gravitational force
$F_{\text{in}}$	Inertial force
$F_d$	Drag force
$F_{\text{em}}$	Electromagnetic force

## Lagrange equation

To derive the **equations of motion**, we started from the Lagrange equation of the system:

$$\frac{d}{dt} \left( \frac{\partial \mathcal{T}}{\partial \dot{\mathbf{u}}} \right) - \frac{\partial \mathcal{T}}{\partial \mathbf{u}} + \frac{\partial \mathcal{D}}{\partial \dot{\mathbf{u}}} + \frac{\partial \mathcal{U}}{\partial \mathbf{u}} = \mathcal{Q}, \text{ where } \mathbf{u} = \begin{bmatrix} z \\ q \end{bmatrix} \quad (1)$$

The energy terms are defined as follows:

$$\begin{aligned} \mathcal{T} &= \frac{1}{2} m \dot{z}^2 + \frac{1}{2} L(z, \dot{q}) \dot{q}^2 \\ \mathcal{D} &= \int_{\dot{z}(\cdot)} \frac{1}{2} C_d A \rho \dot{z}^2 d\dot{z} + \int_{\dot{q}(\cdot)} R(\dot{q}) \dot{q} d\dot{q} \\ \mathcal{U} &= -mgz - qV \\ \mathcal{Q} &= 0 \end{aligned} \quad (2)$$

## Electrical components model

Based on experimental data, we have proposed a model for both the resistance and the coil inductance:

$$\begin{aligned} R &= R(I) = R_0 \\ L &= L(z, I) = L_0 + L_z e^{-a_z z} + L_I \arctan(a_I I - b_I) \end{aligned} \tag{3}$$

The first and second derivatives with respect to ball position and current are:

$$\begin{aligned} \frac{\partial L}{\partial z} &= -a_z L_z e^{-a_z z} & \frac{\partial L}{\partial I} &= \frac{L_I a_I}{1 + (a_I I - b_I)^2} \\ \frac{\partial^2 L}{\partial z^2} &= a_z^2 L_z e^{-a_z z} & \frac{\partial^2 L}{\partial I^2} &= -2 \frac{L_I a_I^2 (a_I I - b_I)}{(1 + (a_I I - b_I)^2)^2} \end{aligned} \tag{4}$$

## Model approximations

In order to simplify the model, some approximations have been considered:

$$\begin{cases} \frac{\partial L}{\partial I} \approx 0 \\ \frac{\partial^2 L}{\partial I^2} \approx 0 \\ \dot{z} \approx 0 \end{cases} \quad (5)$$

Notice that, from successive analysis, these approximations have proven (at least in the range of interest) to be valid.

By applying approximations of Equation (5) to the Lagrange equation (1), we have obtained the following equations of motion:

$$\begin{cases} \dot{z} = v \\ \dot{v} = m^{-1} \left( \frac{1}{2} \frac{\partial L}{\partial z} I^2 + mg \right) \\ \dot{I} = L^{-1} (-RI + V) \end{cases} \quad (6)$$

Model non-linearities are hidden in all the terms relative to the inductance  $L$  and its derivatives.

Despite the applied approximations, the set of Equations (6) is still **able to capture the main dynamics of the system**.

## **Parameters identification**

---

# Optical sensor characterization

A mapping between the output voltage of the optical infrared sensor and the position of the ball has been obtained.

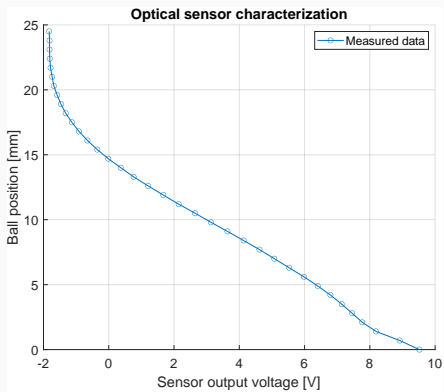


**Figure 4:** Ball position as a function of the sensor output voltage

## Sensors noise analysis

Noises on both the position and current sensors has been analyzed. Classical probability indices<sup>1</sup> have been computed to evaluate the quality of the sensors.

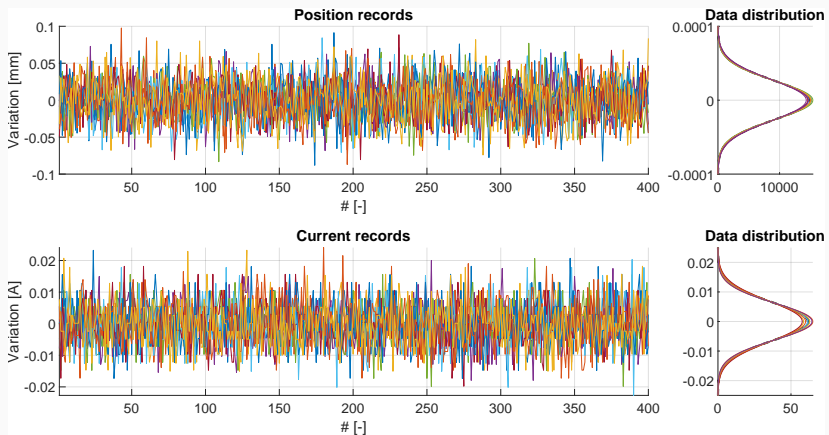


**Figure 5:** Noise analysis for both the position and current sensors

<sup>1</sup>Standard deviation and covariance have been considered.

## Control to Voltage mapping

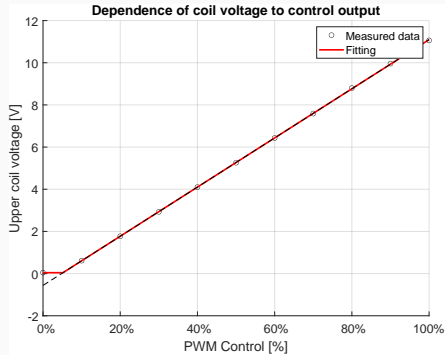


**Figure 6:** Effective coil voltage  $V$  as a function of the control signal  $U$

Mapping between the control signal  $U$  and the effective coil voltage  $V$  has also been evaluated.

$$V = \begin{cases} V_{min} & \text{if } U < U_{min} \\ kU + c & \text{if } U \geq U_{min} \end{cases} \quad (7)$$

## Inductance characterization

As already discussed, we assume  $L(z, I) = L_0 + L_z e^{-azz} + L_I \arctan(a_I I - b_I)$ .

Each of the experimental current transients has been fitted with the following RL circuit model:

$$I(t) = \frac{\Delta V}{R_0} \left( 1 - e^{-\frac{R_0}{L(z,I)} t} \right) \quad (8)$$

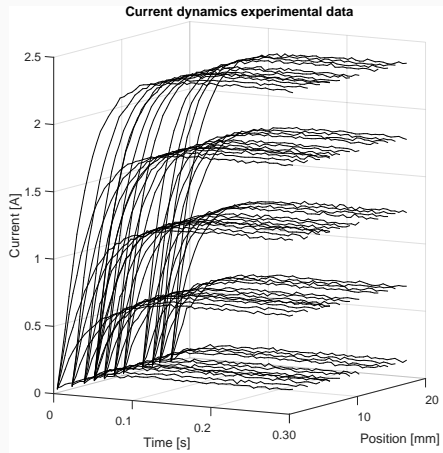


**Figure 7:** (Some) Experimental current transients for different  $z$  (fixed) and  $\Delta V$  applied

## Inductance characterization

As already discussed, we assume  $L(z, I) = L_0 + L_z e^{-azz} + L_I \arctan(a_I I - b_I)$ .

Each of the experimental current transients has been fitted with the following RL circuit model:

$$I(t) = \frac{\Delta V}{R_0} \left( 1 - e^{-\frac{R_0}{L(z,I)} t} \right) \quad (8)$$

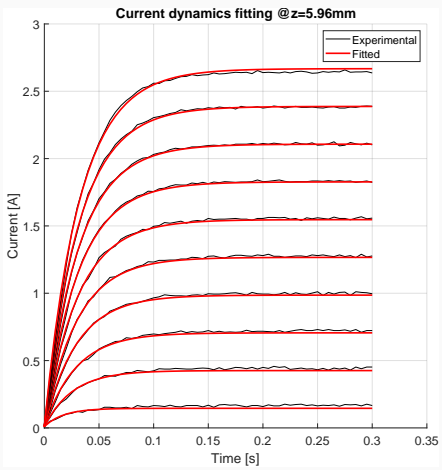


**Figure 7:** Fitted current transients for a given  $z$  (fixed) and different  $\Delta V$  applied

## Inductance characterization

As already discussed, we assume  $L(z, I) = L_0 + L_z e^{-azz} + L_I \arctan(a_I I - b_I)$ .

Repeating the procedure for many couples of  $z$  and  $I$ , a full model for the inductance is obtained.

In the image, black dots represent the previously computed/fitted values of  $L(z, I)$ , while the surface represents the complete inductance model.

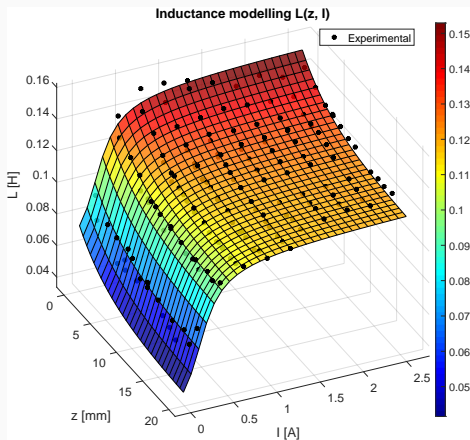
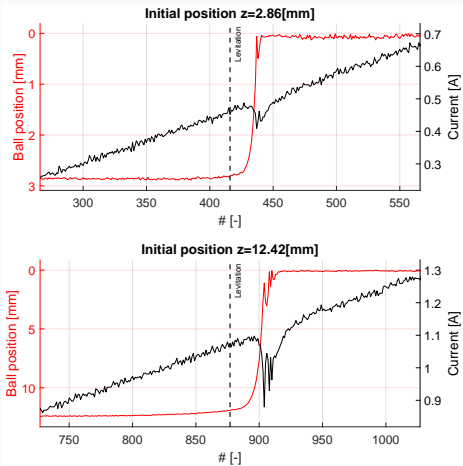


Figure 7: Fitted model for  $L(z, I)$

# Electromagnetic force analysis



**Figure 8:** Current and ball position around the incipient point

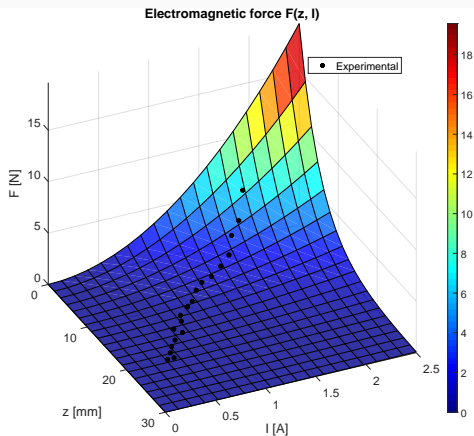
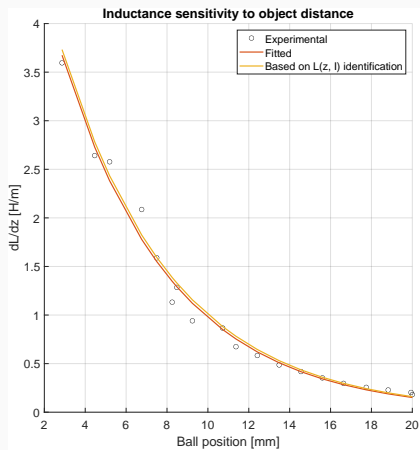
From the equations of motion, we have found  $F_{em} = \frac{1}{2} \frac{\partial L}{\partial z} I^2$ .

Knowing that at the incipient  $F_{em} = mg$ , we can compute  $\frac{\partial L}{\partial z}$  to observe if it's consistent with the previously obtained parameters.

$$\left( \frac{\partial L}{\partial z} = \frac{2mg}{I^2} \right) \Big|_{\text{incipient}} \quad (8)$$

# Electromagnetic force analysis

Force analysis confirmed the validity of the parameters already identified for the inductance model.



As a subsequent result, a complete model for the electromagnetic force is also obtained.

## Identified parameters

All the identified parameters are listed in the following tables:

Parameter	Value	Unit	Parameter	Value	Unit
$m$	$60.54 \cdot 10^{-3}$	kg	$L_0$	$6.54 \cdot 10^{-2}$	H
$V_{min}$	$4.30 \cdot 10^{-2}$	V	$a_z$	$1.59 \cdot 10^2$	1/m
$U_{min}$	$5.18 \cdot 10^{-2}$	MU	$L_z$	$4.04 \cdot 10^{-2}$	H
$k$	$1.16 \cdot 10^1$	V/MU	$a_I$	5.30	-
$c$	$-5.60 \cdot 10^{-1}$	V	$b_I$	1.04	A
$R_0$	4.17	$\Omega$	$L_I$	$3.29 \cdot 10^{-2}$	H

Table 1: Model's identified parameters

Sensor	Standard deviation	Covariance
Infrared	$2.68 \cdot 10^{-5}$ [m]	$7.21 \cdot 10^{-10}$ [ $m^2$ ]
Current	$6.48 \cdot 10^{-3}$ [A]	$4.21 \cdot 10^{-5}$ [ $A^2$ ]

Table 2: Sensors' noise parameters.

---

<sup>0</sup>MU stands for 'Machine Unit'

## **Model Analysis**

---

## Linearization and Transfer function $G(s)$

Considering linearization around the position of 10[mm], the following state-space representation of the system is obtained:

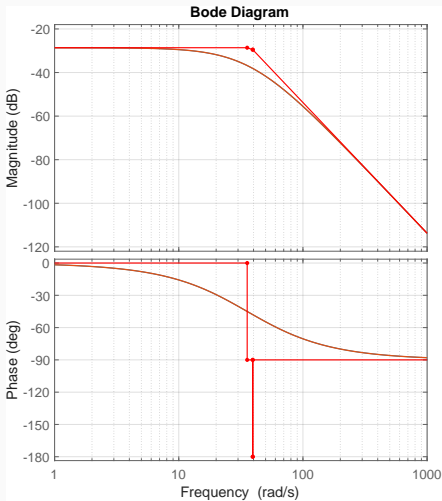
$$A = \begin{bmatrix} 0 & 1 & 0 \\ 1555 & 0 & -20.63 \\ 0 & 0 & -35.55 \end{bmatrix} \quad B = \begin{bmatrix} 0 \\ 0 \\ 99.41 \end{bmatrix} \quad (8)$$

$$C = \begin{bmatrix} 1 & 0 & 0 \end{bmatrix} \quad D = \begin{bmatrix} 0 \end{bmatrix} \quad (9)$$

Based on this, the transfer function  $G(s)$  of the system is given by:

$$G(s) = C(sI - A)^{-1}B + D = \frac{-2051}{s^3 + 35.56s^2 - 1555s - 5.53 \cdot 10^4} \quad (10)$$

## Stability analysis



The Bode plot shows that the system is unstable, as the gain margin is negative.

Instability is also confirmed by the poles of the system:

$$\text{eig}(A) = \begin{cases} 39.44 \\ -39.44 \\ -35.56 \end{cases} \quad (11)$$

Figure 8: Bode plot for the transfer function  $G(s)$ .

## Stability analysis

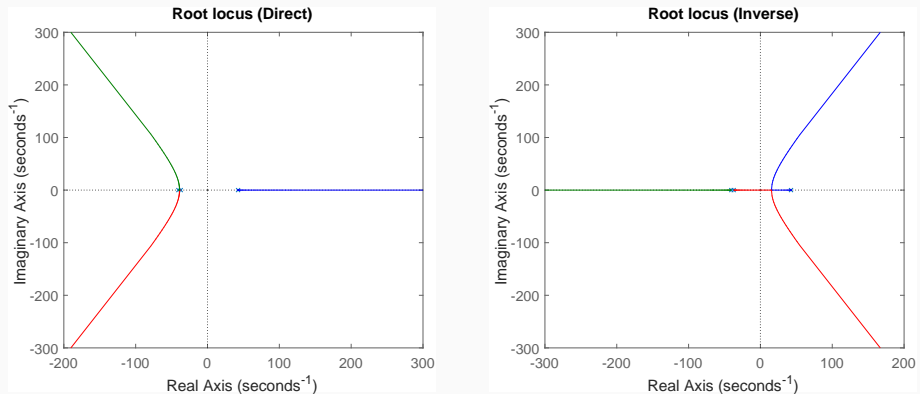


Figure 9: Root Locus plot with positive and negative proportional feedback control.

Luckily, the system is controllable and reachable, as the rank of both the controllability and reachability matrices is equal to the number of states.

We can now move on to the design of estimators and controllers for the system.

## **Estimators and Filters Design**

---

Many control strategies require the knowledge of all the system states. For this reason, some state estimators have been designed together with some filters to reduce the noise in the measurements.

- **Low-pass filter;**
- **Luenberger observer.**
- **Kalman filter.**
- **Extended Kalman filter.**

## Low-pass filter

A first order low-pass filter has been implemented:

$$G(s) = \frac{1}{\tau s + 1} \quad (12)$$

where the time constant of the filter is:

$$\tau = \frac{1}{\omega_c} = \frac{1}{200} = 5ms \quad (13)$$

where  $\omega_c = 10\omega_n \approx 200rad/s$  is the cut-off frequency, and  $\omega_n = \frac{2\pi}{T_p} \approx 20rad/s$  is the bandwidth of the system. Filter delay can also be computed as:

$$\phi = -\text{arctan}(\omega_c \tau) = -5.7^\circ \quad (14)$$

In order to estimate the state of the system<sup>1</sup>, the Luenberger Observer has been implemented considering by chance the following eigenvalues:

$$\text{eig}(A - LC) = \begin{bmatrix} -500 \\ -400 \\ -400 \end{bmatrix} \quad (15)$$

Leading to the following observer gain:

$$L = \begin{bmatrix} 900.00 & 0 \\ 201555.32 & -20.63 \\ 0 & 364.44 \end{bmatrix} \quad (16)$$

---

<sup>1</sup>For all the estimators proposed, we consider to have both  $z$  and  $I$  as measurements from the system and estimate  $v$ .

Another estimation of the state of the system can be made with the Kalman filter, where process and noise covariance matrices are given by:

$$Q = \begin{bmatrix} 0 & 0 & 0 \\ 0 & 10 & 0 \\ 0 & 0 & 10 \end{bmatrix} \quad R = \begin{bmatrix} 7.21 \cdot 10^{-10} & 0 \\ 0 & 4.21 \cdot 10^{-5} \end{bmatrix} \quad (17)$$

The Kalman gain  $K$  is then obtained:

$$K = \begin{bmatrix} 487 & -0 \\ 119069 & -15 \\ -911 & 453 \end{bmatrix} \quad (18)$$

the poles of the observer are given by:

$$\text{eig}(A - KC) = \begin{bmatrix} -243.94 + 240.82i \\ -243.94 - 240.82i \\ -488.87 + 0i \end{bmatrix} \quad (19)$$

The extended Kalman filter does a recursive state estimation for our nonlinear systems.

The design parameters are the same as the Kalman filter with the key difference that the gain matrix  $K_k$  is computed online at each time step  $t_k$  based on the current state estimate  $\hat{x}_k$ .

## **Controllers design**

---

The control of the system is achieved by designing different controllers:

- **PIDs controller;**
- **LQs controller;**
- **MPC controller.**

- **Problem:** **Integrator windup** occurs when the actuator saturates, causing uncontrolled growth of the integral term. This degrades the rise time and can lead to a **higher overshoot**.
- **Solution: Conditional Integration.** The controller output is compared with the actuator limits. If saturation is detected and error accumulates, the integrator is turned off.

The gain parameters reported below have been estimated firstly considering the Bode diagram, and subsequently analyzing the Root Locus:

$$K_p = -150 \quad K_i = -450 \quad K_d = -6.82 \quad (20)$$

## PID with Gain Scheduling

- PID controller tuned at a series of **steady-state operating points**.
- The sphere's movement space is divided into **multiple points**, and the system is **linearized** locally at each operating point.
- Controller gains are **optimized** for each operating condition.
- Gain curves **gradually vary** between points.

$z[mm]$	$K_p$	$K_i$	$K_d$
5	-102	-306	-4.64
8	-136	-408	-6.18
12	-183	-550	-8.34
16	-250	-750	-11.4
20	-342	-1030	-15.5

Table 3: Look up table for the PID gain scheduling

## LQR with tracking capabilities

The **LQR with tracking capabilities**, extends the classical LQR framework to manage systems where the goal is not only to stabilize the system but also to ensure it follows a desired trajectory.

For the matrix  $\mathbf{Q}$ , particular attention is given to the values affecting the position of the sphere, with moderate emphasis on the current state. The matrix  $\mathbf{R}$  is estimated based on literature parameters.

- Design parameters:

$$\mathbf{Q} = \begin{bmatrix} 25 \cdot 10^3 & 0 & 0 \\ 0 & 0 & 0 \\ 0 & 0 & 16 \cdot 10^{-2} \end{bmatrix} \quad \mathbf{R} = 0.5 \quad (21)$$

- Computed feedback gain:

$$\mathbf{K} = \begin{bmatrix} -371.72 & -7.53 & 1.53 \end{bmatrix} \quad (22)$$

The LQI (Linear Quadratic Integrator) is an extension of LQR that incorporates integral states to improve reference tracking and disturbance rejection. By adding integration of tracking error, LQI reduces persistent errors between the system and reference, improving control accuracy.

- Design parameters:

$$\mathbf{Q} = \begin{bmatrix} 25 \cdot 10^3 & 0 & 0 & 0 \\ 0 & 0 & 0 & 0 \\ 0 & 0 & 16 \cdot 10^{-2} & 0 \\ 0 & 0 & 0 & 10^6 \end{bmatrix} \quad \mathbf{R} = 0.5 \quad (23)$$

- Computed feedback gain:

$$\mathbf{K} = \begin{bmatrix} -513.31 & -9.19 & 1.71 & 4472.13 \end{bmatrix} \quad (24)$$

**Model Predictive Control (MPC)** is an advanced control strategy that optimizes system performance by continuously reinitializing the control procedure.

- Based on a linear system model.
- Constraints are applied.
- Computationally less expensive compared to nonlinear MPC.

$$\begin{aligned} \text{Prediction Horizon} &= 0.1 \text{ s} \\ \text{Control Horizon} &= 0.01 \text{ s} \end{aligned} \tag{25}$$

Constraints on position and control are applied, as shown in the table below:

Variable	Max	Min
Position	20 mm	0 mm
Control	1	0

**Table 4:** Constraints for the MPC controller

## **Results**

---

Different reference signals have been used to evaluate the controllers' performance, including:

- **Multistep (stars and up & down)**: a sequence of equally spaced step inputs ( $1[mm]$  or  $2[mm]$  in amplitude) to assess the controller's response to abrupt set-point changes and its steady-state performance across various set-points.
- **Sinusoidal (discrete)**: a sinusoidal shape (period  $2[s]$ , amplitude  $2[mm]$ ), but represented as a sequence of discrete steps, to evaluate the controllers' performance in tracking a periodic signal.

All the results here presented are obtained using a Kalman filter to estimate and/or filter the system's state.

# Controller comparison

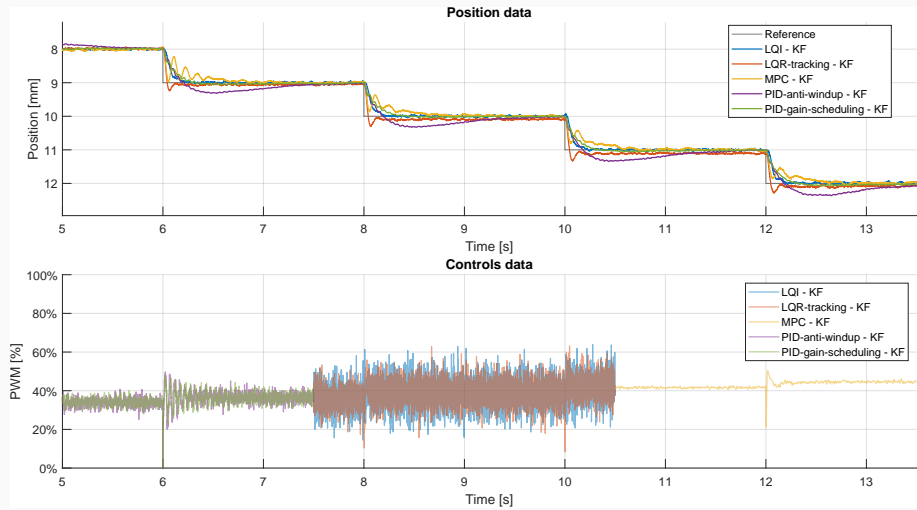


Figure 10: Comparison of controllers with multistep stairs reference using KF

# Controller comparison

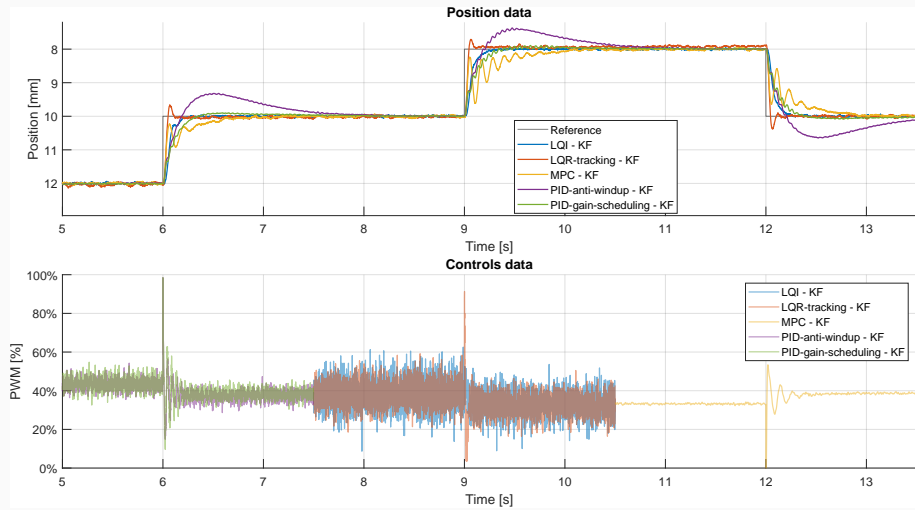


Figure 11: Comparison of controllers with multistep up & down reference using KF

# Controller comparison

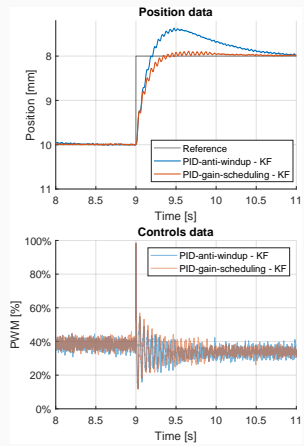


Figure 12: PIDs, LQs, MPC with multistep up reference using KF

# Controller comparison

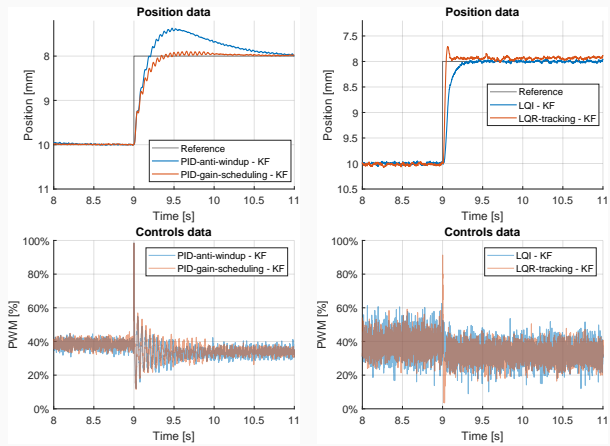


Figure 12: PIDs, LQs, MPC with multistep up reference using KF

# Controller comparison

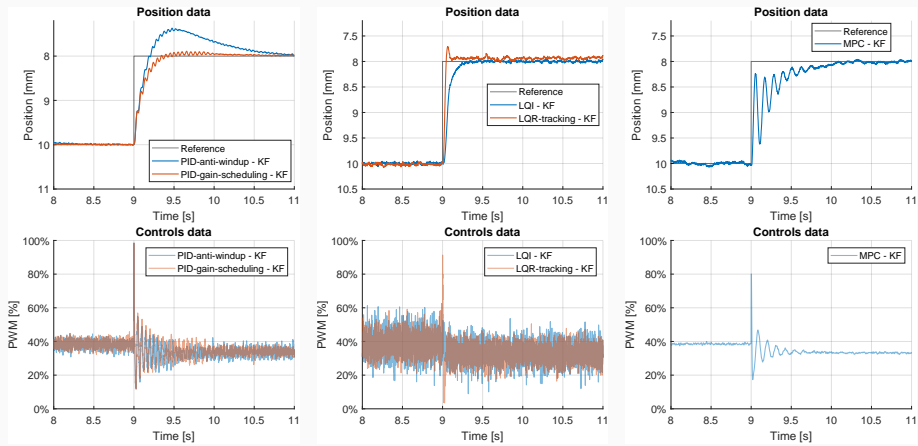
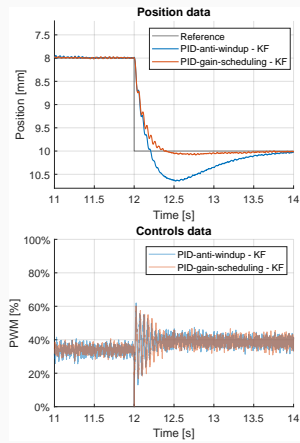


Figure 12: PIDs, LQs, MPC with multistep up reference using KF

# Controller comparison



**Figure 13:** PIDs, LQs, MPC with multistep up & down (down) reference using KF

# Controller comparison

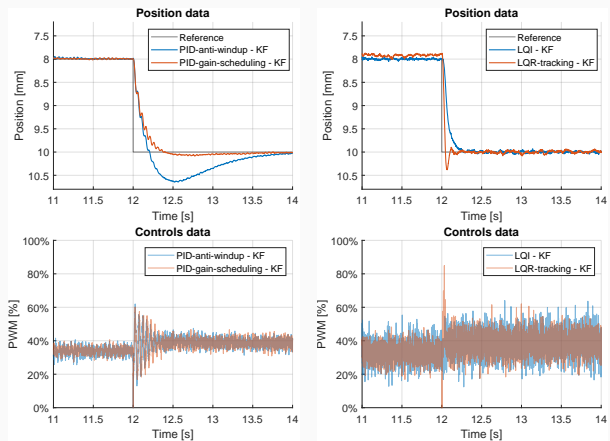


**Figure 13:** PIDs, LQs, MPC with multistep up & down (down) reference using KF

# Controller comparison

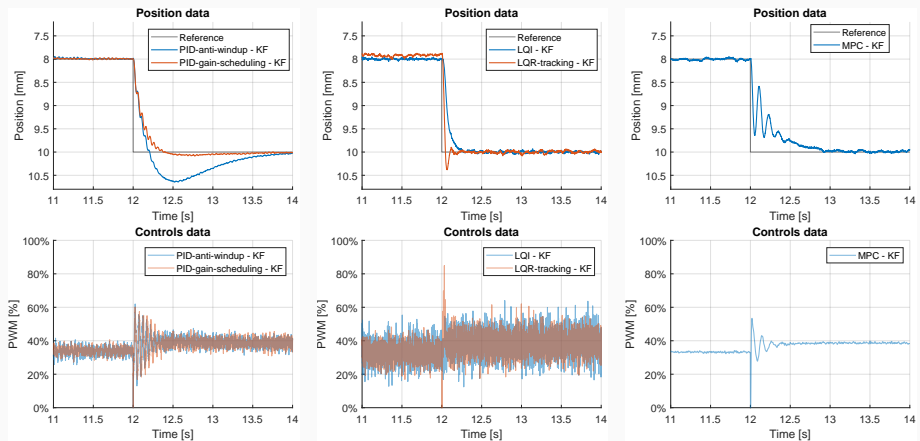


**Figure 13:** PIDs, LQs, MPC with multistep up & down (down) reference using KF

# Controller comparison

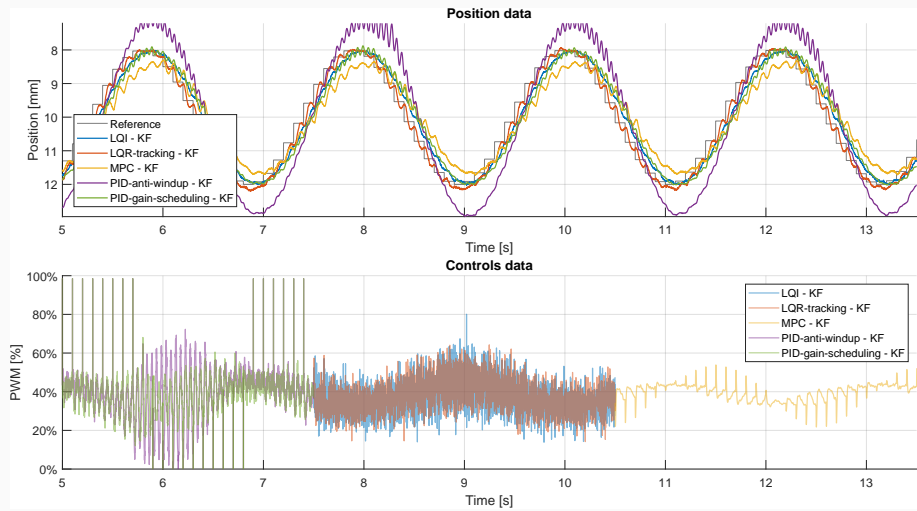
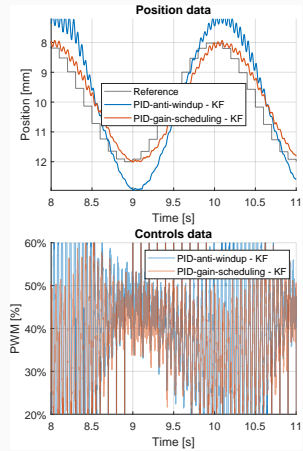


Figure 14: Comparison of controllers with sinusoidal slow reference using KF

## Controller comparison



**Figure 15:** PIDs, LQs, MPC with sinusoidal fast reference using KF

# Controller comparison

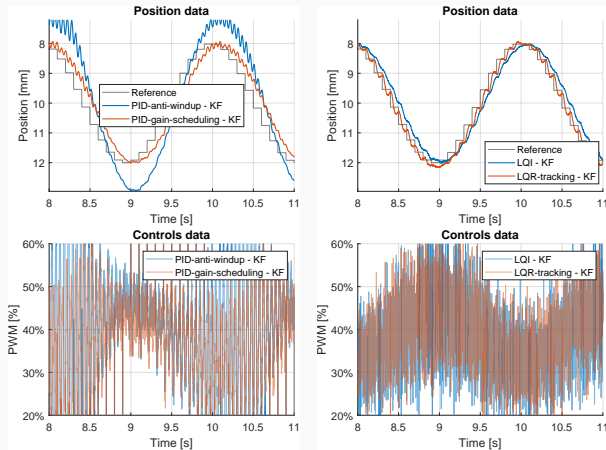


Figure 15: PIDs, LQs, MPC with sinusoidal fast reference using KF

# Controller comparison

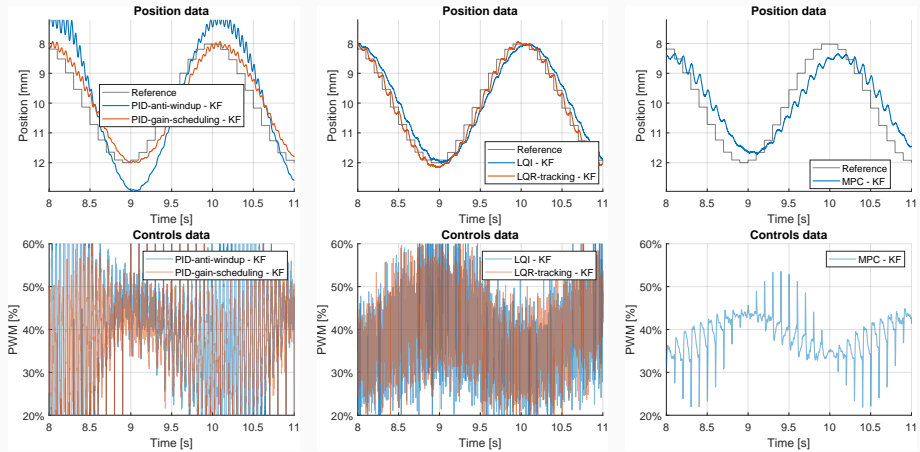


Figure 15: PIDs, LQs, MPC with sinusoidal fast reference using KF

## Controller considerations

Overall, from the results obtained, we can draw the following considerations:

Controller	Reactivity	Precision	Stability	Control
<b>PID Anti-windup</b>	Slow	Good (steady-state)	Moderate	High noise
<b>PID Gain Scheduling</b>	Good	Good	Good	High noise
<b>LQR Tracking</b>	Very high	High	Good	High noise
<b>LQI</b>	Very high	Excellent	Excellent	High noise
<b>MPC</b>	High	Good	Good	Excellent

**Table 5:** Controller Comparison

To compare filters and estimators, an LQR tracking was used as a controller and a continuous sinusoidal reference signal with a period of  $2[s]$  and amplitude of  $2[mm]$  was used as a reference signal.

Regarding the estimators, only position and current measurements were used as input, while velocity was estimated.

# Filter & Estimator comparison

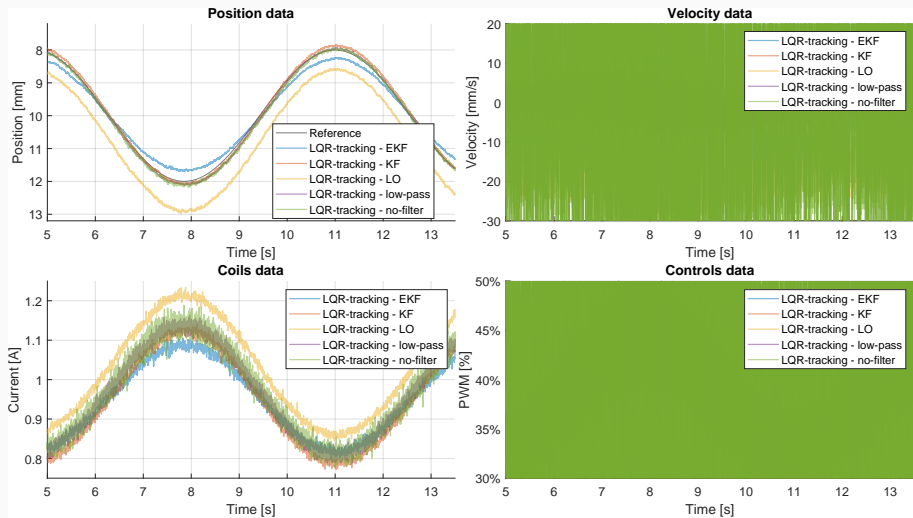


Figure 16: Comparison of filter using an LQR tracking with sinusoidal slow reference

# Filter & Estimator comparison

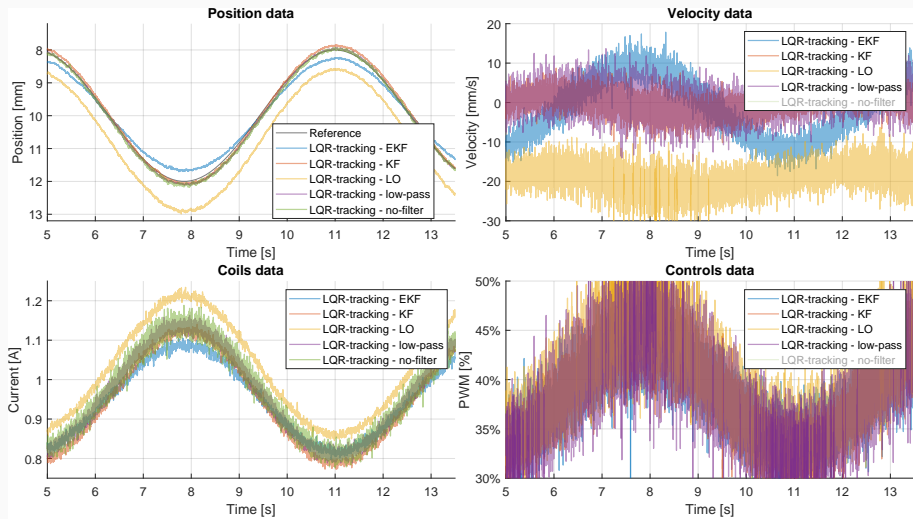
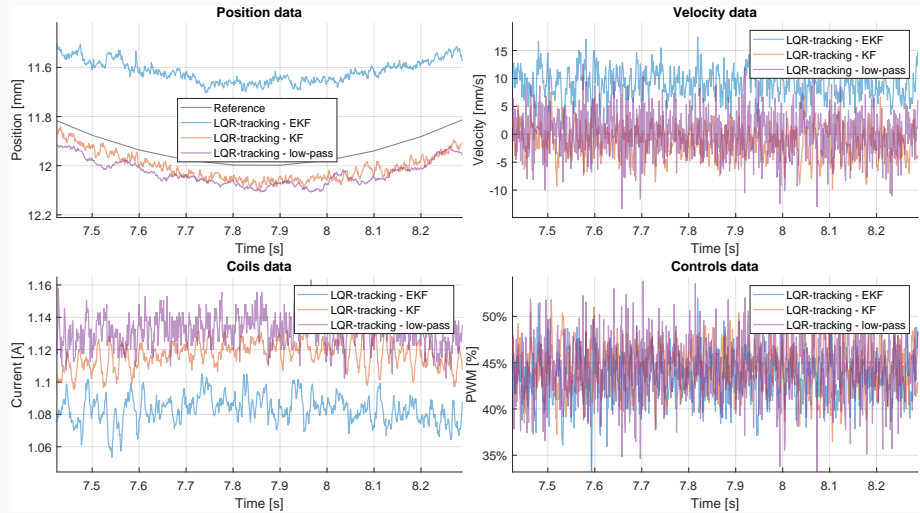


Figure 17: Comparison of filter using an LQR tracking with sinusoidal slow reference

# Filter & Estimator comparison



**Figure 18:** Comparison of no filter, low pass, KF using an LQR tracking with sinusoidal slow reference

## Filter & Estimator considerations

Overall, from the results obtained, we can draw the following considerations:

Filter/Estimator	Noise reduction	Estimation accuracy	Delay
No filter	-	-	Absent
Low-pass filter	Good	-	Minimal
Luenberg Observer	Optimal	Extremely inaccurate	Absent
Kalman filter	Optimal	Good	Absent
Extended Kalman filter	Optimal	Inaccurate	Absent

Table 6: Filters and Estimators comparison

These results highlight the need for further fine-tuning of the **EKF**.

## **Conclusions**

---

## Conclusions

Ball levitation was achieved by implementing various control strategies and filtering methods, and the performance of each was evaluated through simulations and real-world experiments.

Based on the results obtained, we can state that:

- For **control strategies**, the **MPC Controller** emerged as the most effective, providing accurate control with minimal oscillations and high stability.
- Regarding **filtering & estimator methods**, the **Kalman Filter** demonstrated the best performance, ensuring accurate state estimation and disturbance rejection.

## Future work

For future work, we suggest the implementation of control techniques that consider the full nonlinear model of the system, such as:

- **Nonlinear Model Predictive Control**
- **Feedback Linearization**
- **Backstepping controllers**

These methods could improve the system's robustness and adaptability, offering better performance in handling larger disturbances, nonlinearities, and uncertainties.

## References i

-  P. Balko and D. Rosinova.  
**Modeling of magnetic levitation system.**  
pages 252–257, 06 2017.
-  INTECO.  
**Magnetic levitation systems — inteco.**  
<https://www.inteco.com.pl/products/magnetic-levitation-systems/>,  
2014.  
[Online; accessed 26-September-2024].

**Questions?**

**Thank you!**